

Congested Urban Networks Tend to Be Insensitive to Signal Settings: Implications for Learning-Based Control

Jorge Laval^{a,*}, Hao Zhou^a

^a*School of Civil and Environmental Engineering, Georgia Institute of Technology, Atlanta, United States*

Abstract

This paper highlights several properties of large urban networks that can have an impact on machine learning methods applied to traffic signal control. In particular, we show that the average network flow tends to be independent of the signal control policy as density increases. This property, which so far has remained under the radar, implies that deep reinforcement learning (DRL) methods becomes ineffective when trained under congested conditions, and might explain DRL's limited success for traffic signal control. Our results apply to all possible grid networks thanks to a parametrization based on two network parameters: the ratio of the expected distance between consecutive traffic lights to the expected green time, and the turning probability at intersections. Networks with different parameters exhibit very different responses to traffic signal control. Notably, we found that no control (i.e. random policy) can be an effective control strategy for a surprisingly large family of networks. The impact of the turning probability turned out to be very significant both for baseline and for DRL policies. It also explains the loss of symmetry observed for these policies, which is not captured by existing theories that rely on corridor approximations without turns. Our findings also suggest that supervised learning methods have enormous potential as they require very little examples to produce excellent policies.

Keywords: Traffic signal control, machine learning, deep reinforcement learning

1. Introduction

Congested urban networks have long been considered to behave chaotically and to be very unpredictable, with output flows being hypersensitive to the input demand (Daganzo, 1996, 1998, Nair et al., 2001, Adewumi et al., 2016). This apparent complexity has led to the development of numerous signal control algorithms, mathematical programs and learning-based control methods to optimize network performance (see e.g., Khamis and Gomaa, 2014, Chu et al., 2016, Xu et al., 2018, Ge et al., 2019, Wei et al., 2019, Tan et al., 2019, Gong et al., 2019). Although operational improvements have been shown in these references, they mostly correspond to light traffic conditions or very specific small networks. And success has been limited when it comes to outperforming greedy benchmarks even under lightly congested conditions (Belletti et al., 2017).

The recent empirical verification of the existence of a network-level Macroscopic Fundamental Diagram (MFD) suggests a different story, however. The network MFD has its origins in Godfrey (1969) as a way of describing the traffic flow of urban networks at an aggregate level, and has been used in the past as a concise way of displaying network simulation output (Smeed, 1967, Herman and Prigogine, 1979, Herman and Ardekani, 1984, Mahmassani et al., 1984). The MFD gives the average flow on a network as a function of the number of vehicles inside the network, arguably independently of trip origins and destinations, and route choice. This robustness strongly suggests that signal timing effects might be limited. We argue here that the main cause of our struggles to control congested urban networks is not complexity but simplicity, as suggested by the MFD. While small networks might exhibit high

*Corresponding author

Email address: jorge.laval@ce.gatech.edu (Jorge Laval)

¹790 Atlantic Dr NW, Atlanta, GA, 30313

throughput variations (Daganzo, 1998), we show here that large congested networks tend to produce a throughput that is quite predictable, and which cannot be controlled in congestion because it tends to be independent of the signal control policy. We call this property the “congested network property”.

An early indication of this property, which unfortunately remained under the radar all these years, can be traced back to the work of Robert Herman and his group in the mid-eighties around the two-fluid model (Herman and Ardekani, 1984, Mahmassani et al., 1985, 1990). Although not mentioned explicitly in these references, some of the figures reveal a significant insensitivity of network performance with respect to signal control ². They also find that block length positively influences network throughput. Notice that these results are based on the microscopic model NETSIM over an idealized grid network with identical block lengths, which might explain why the authors were reluctant to highlight the insensitivity to traffic signal control.

The lack of study of the congested network property is unfortunate because it means, based on our results, that potentially all the DRL methods proposed in the literature to date are unable to learn effective control policies as soon as congestion appears on the network. In fact, Camponogara and Kraus (2003) showed that at above the critical density the resulting DRL policies deteriorate significantly. The congested network property might also explain the limited success of DRL for traffic signal control, rather than the current explanation in the literature of non-stationary and/or non-Markovian (Choi et al., 2000, Da Silva et al., 2006) behavior of the environment.

A more recent indication of this property can be found in Laval and Castrillón (2015), who show that the network MFD can be well approximated by a function of only three measurable network parameters:

$$\lambda \propto E(\text{block length})/E(\text{green time}), \quad (1a)$$

$$\delta = COV(\text{block length}) \quad \text{and} \quad \rho = E(\text{red time})/E(\text{green time}) \quad (1b)$$

where $E(\cdot)$, $COV(\cdot)$ stand for expectation and coefficient of variation, respectively, and block length refers to the distance between consecutive traffic lights. But $\rho = 1$ when we consider all travel directions, such as in this paper, and therefore can be dropped from the formulation. This strongly suggests that signal timing might be irrelevant when considering all directions of travel and only affects network performance by the average green time across all directions of travel. As we will show in this paper, it turns out that the parameter δ that regulates the variance of block lengths affects the MFD only slightly, and thus can also be dropped from the formulation. The only variable left is λ , a measure of the propensity of the network to experience spillbacks, which waste capacity. It was shown in Laval and Castrillón (2015) that $\lambda < 1$ is the “short-block condition”, i.e. the network becomes prone to spillback, which can have a severe effect on capacity.

Here we show that the turning probability at intersections is also a key variable that significantly affects the MFD. Unfortunately, its impacts are not well understood in the literature. Daganzo et al. (2011) found the breakdown time for a one-way street network seems to be insensitive to the probability of turning, but Gayah et al. (2014) found that a fixed turning probability of 0.2 lead a one-way street network towards gridlock more quickly than with random turning. To make matters worse, existing MFD estimation methods are based on arterial corridors without turning movements, and have been used as an approximation to the MFD of the whole network. This implies assuming that turning movements do not affect the MFD, which is not the case as will be shown here.

We will see shortly see that a gap in the DRL literature appears to be a consistent analysis of the different aspects of large traffic flow networks that influence the performance of DRL methods. For example, it is not clear if and how network congestion levels affect the learning process, nor if other machine learning methods are effective, nor if current findings also apply to large networks. This paper is a step in this direction, where we examine the simplest possible DRL setup in order to gain some insight on how the optimal policy changes with respect to different configurations of the learning framework.

In this paper we will (i) provide additional evidence for the congested network property by expanding the experiments in Herman and Ardekani (1984), Mahmassani et al. (1985, 1990) to all grid network topologies, (ii) unveil additional properties such as loss of symmetry, overlapping and detaching, and (iii) analyze how these properties affect the performance of machine learning methods applied to signal control. Towards this end, the remainder of the

²For example, figures 9a, 10a and 11a in Williams et al. (1985) show that providing signal progression does not significantly improve the average speed on the network; figures 5.10 and 5.13 in Mahmassani et al. (1985) show that signal offset has no discernible influence on network throughput.

paper is organized as follows. We start with the background section on the MFD, DRL and a survey of related work. Then, we define the problem setup and apply it to a series of experiments that highlight the main properties found here. Finally, the paper concludes with a discussion and outlook section.

2. BACKGROUND

2.1. MFD estimation

As mentioned in the introduction the Macroscopic Fundamental Diagram (MFD) for a given traffic network describes the relationship between traffic variables averaged across all *lanes* in the network. The main requirement for a well-defined MFD is that congestion be homogeneously distributed across the network, i.e. there must be no "hot spots" in the network. For analytical derivations it is often also assumed that each *lane* of the network obeys the kinematic wave model (Lighthill and Whitham, 1955, Richards, 1956) with common fundamental diagram (Daganzo and Geroliminis, 2008, Laval and Castrillón, 2015). In this way, upper bounds for the MFD have been found using the method of cuts in the case of homogeneous networks (Daganzo and Geroliminis, 2008). In a flow-density diagram a "cut" is a straight line with slope (wave speed) corresponding to the average speed of a moving observer and intercept given by the maximum passing rate the observer would measure. By varying the observer speed one obtains a series of cuts whose lower envelope gives an approximation of the MFD. For general networks, Laval and Castrillón (2015) introduces the stochastic method of cuts and shows that (the probability distribution of) the MFD can be well approximated by a function of the three parameters in (1). In particular to this paper, the cuts' wave speed produced by this theory for extreme free-flow, u_0 , and extreme congestion, $-w_0$, are given by:

$$u_0 = w_0 = \frac{4\lambda}{\delta^2 + 2\lambda + 1}. \quad (2)$$

after using $\rho = 1$ in equation (17b) of Laval and Castrillón (2015).

Notice that these estimation methods give the MFD of an arterial corridor without turning movements, and have been used as an approximation to the MFD of the whole network. This implies assuming that turning movements do not affect the MFD, which is not the case as will be shown here.

2.2. Reinforcement learning

The use of deep neural networks within Reinforcement Learning algorithms has produced important breakthroughs in recent years. These deep reinforcement learning (DRL) methods have outperformed expert knowledge methods in areas such as arcade games, backgammon, the game Go and autonomous driving (Mnih et al., 2015, Silver et al., 2017, Chen et al., 2019). In the area of traffic signal control numerous DRL control methods have been proposed both for isolated intersections (Li et al., 2016, Genders and Razavi, 2016) and small networks (Chu and Wang, 2015, Chu et al., 2019, Tan et al., 2019, Ge et al., 2019). The vast majority of these methods have been trained with a single (dynamic) traffic demand profile, and then validated using another one, possibly including a surge (Ge et al., 2019).

In the current signal control DRL literature the problem is treated, invariably, as an episode process, which is puzzling given that the problem is naturally a continuing (infinite horizon) one. Here, we adopt the *continuing* approach to maximize the long-term average reward. We argue that in signal control there is no terminal state because the process actually goes on forever. And what may appear as a terminal state, such as an empty network, cannot be considered so because it is not achieved through the correct choice of actions but by the traffic demand, which is uncontrollable. An explanation for this puzzling choice in the literature might be that DRL training methods for episodic problems have a much longer history and our implemented in most machine learning development frameworks. For continuing problems this is not unfortunately the case, and we propose here the training algorithm REINFORCE-TD, which is in the spirit of REINFORCE with baseline (Williamms, 1988) but for continuing problems. To the best of our knowledge, this extension of REINFORCE is not available in the literature.

Reinforcement learning is typically formulated within the framework of a *Markov decision process* (MDP). At discrete time step t the environment is in state $S_t \in \mathcal{S}$, the agent will choose and action $A_t \in \mathcal{A}$, to maximize a function of future rewards $R_{t+1}, R_{t+2} \dots$ with $R_- : \mathcal{S} \times \mathcal{A} \rightarrow \mathfrak{R}$. There is a state transition probability distribution $P(s', r|s, a) = \Pr(S_t = s', R_t = r|S_{t-1} = s, A_{t-1} = a)$ that gives the probability of making a transition from state s to state s' using action a is denoted $P(s, a, s')$, and is commonly referred to as the "model". The model is *Markovian*

since the state transitions are independent of any previous environment states or agent actions. For more details on MDP models the reader is referred to Bellman (1957), Bertsekas (1987), Howard (1960), Puterman (1994)

The agent’s decisions are characterized by a stochastic **policy** $\pi(a|s)$, which is the probability of taking action a in state s . In the continuing case the agent seeks to maximize the *average reward*:

$$\eta(\pi) \equiv \lim_{T \rightarrow \infty} \frac{1}{T} \sum_{t=1}^T E_{\pi} [R_t] \quad (3)$$

The term E_{π} means that the expected value (with respect to the distribution of states) assumes that the policy is followed.

In the case of traffic signal control for large-scale grid network, methods based on transition probabilities are impractical because the state-action space tends to be too large as the number of agents increases. An alternative approach that circumvents this *curse of dimensionality* problem—the approach we pursue here—are “policy-gradient” algorithms, where the policy is parameterized as $\pi(a|s; \theta)$, $\theta \in \mathcal{R}^m$, typically a neural network. Parameters θ are adjusted to improve the performance of the policy π by following the gradient of cumulative future rewards, given by the identity

$$\nabla \eta = E_{\pi} [G_t \nabla_{\theta} \log \pi(a|s)] \quad (4)$$

as shown in Sutton (1999) for both continuing and episodic problems. In continuing problems cumulative rewards G_t are measured relative to the average cumulative reward:

$$G_t = \sum_{i=t+1}^{\infty} (R_i - \eta(\pi)) \quad (5)$$

and is known as the *differential return*.

2.3. Related work

The existing literature is split between two approaches for formulating the large-scale traffic control problem, either a centralized DRL algorithm or a decentralized method with communication and cooperation among multi-agents. The centralized approach (Genders and Razavi, 2016, Li et al., 2016, Chu et al., 2016) adopts a single-agent and tries to tackle the high-dimensional continuous control problem by memory replay, dual networks and advantage actor-critic (Lillicrap et al., 2015, Mnih et al., 2015). The decentralized method takes advantage of multiple agents and usually requires the design of efficient communication and coordination to address the limitation of partial observation of local agents. Current studies (Khamis and Gomaa, 2014, Wei et al., 2019, Tan et al., 2019, Gong et al., 2019) often decompose the large network into small regions or individual intersections, and train the local-optimum policies separately given reward functions reflecting certain level of cooperation with neighboring agents. How to incorporate those communication information to help design the reward function for local agents remains an open question.

The environment modeling, state representation and reward function design are key ingredients in DRL. For the environment emulator, most studies use popular microscopic traffic simulation packages such as AIMSUN or SUMO. Recently, FLOW (Khetarpal et al., 2018) has been developed as a computational framework integrating SUMO with some advanced DRL libraries to implement DRL algorithm on ground traffic scenarios. Vinitzky et al. (2018) provided a benchmark for major traffic control problems including the multiple intersection signal timing. There also exist studies (Chu and Wang, 2015, Arel et al., 2010, Ge et al., 2019) adopting methods to use self-defined traffic models as the environment. Complementary to those microscopic simulation packages, macroscopic models are able to represent the traffic state using cell or link flows. The advantage of macroscopic models is twofold: i) reducing complexity in state space and computation ii) being compatible with domain knowledge from traffic flow theory such as MFD theory.

Expert knowledge has been included in some studies to reduce the scale of the network control problem. In Xu et al. (2018), critical nodes dictating the traffic network were identified first before the DRL was implemented. The state space can be remarkably reduced. MFD theory cannot provide sufficient information to determine the traffic state of a network. For instance, Chu and Wang (2015) successfully integrated the MFD with a microscopic simulator to constrain the searching space of the control policies in their signal design problem. They defined the reward as the trip completion rate of the network, and simultaneously enforcing the network to remain under or near the critical



Figure 1: CA Rule 184: The top row in each of the eight cases shows the the neighborhood values (c_{i-1}, c_i, c_{i+1}) and the updated c_i in the bottom row.

density. The numerical experiments demonstrated that their policy trained by the integration of MFD yields a more robust shape of the MFD, as well as a better performance of trip completion maximization, compared to that of a fixed and a greedy policy.

While most of the related studies on traffic control only focus on developing effective and robust deep learning algorithms, few of them have shown traffic considerations, such as the impact of traffic density. The learning performance of RL-based methods under different densities have not been sufficiently addressed. To the best of our knowledge, Camponogara and Kraus (2003) is the only study which trained a RL policy for specific and varied density levels, but unfortunately their study only accounted for free-flow and mid-level congestion. Dai et al. (2011) classified the traffic demand into four vague levels and reported that inflow rates at 1000 and 1200 veh/h needed more time for the algorithm to show convergence. But they did not report network density, nor try more congested situations nor discussed why the converging process has been delayed. Most studies only trained RL methods in non-congestion conditions, Ge et al. (2019) adopted the Q-value transfer algorithm (QTCDQN) for the cooperative signal control between a simple 2*2 grid network and validated the adaptability of their algorithm to dynamic traffic environments with different densities, such as the the recurring congestion and occasional congestion.

It can be seen that most recent studies focus on developing effective and robust multi-agent DRL algorithms to achieve coordination among intersections. The number of intersections in those studies are usually limited, thus their results might not apply to large networks. Although the signal control is indeed a continuing problem, it has been always modeled as an episodic process. From the perspective of traffic considerations, expert knowledge has only been incorporated in down-scaling the size of the control problem or designing novel reward functions for DRL algorithm. Few studies have tested their methods on a full spectrum of traffic demands, the learning performance under different traffic densities, especially the congestion regimes, has not been fully explored.

3. The simulation environment

The traffic flow model used in this paper is the kinematic wave model (Lighthill and Whitham, 1955, Richards, 1956) with a triangular flow-density fundamental diagram, which is the simplest model able to predict the main features of traffic flow. The shape of the triangular fundamental diagram is irrelevant due to a symmetry in the kinematic wave model whereby flows and delays are invariant with respect to linear transformations, and renders the kinematic wave model parameter-free; see Laval and Chilukuri (2016) for the details. This allows us to use an isosceles fundamental diagram where both the free-flow speed and the wave speed are both equal to 1. This scaling implies that the saturation flow is 1/2 and the jam density is 1.

This fundamental diagram in combination with a cellular automaton (CA) implementation of the kinematic wave model, produces its most computationally efficient numerical solution method: Elementary CA Rule 184 (Wolfram, 1984). In a CA model, each lane of the road is divided into small cells $i = 1, 2, \dots, \ell$ the size of a vehicle jam spacing, where cell ℓ is the most downstream cell of the lane. The value in each cell, namely c_i , can be either “1” if a vehicle is present and “0” otherwise. The update scheme for CA Rule 184, shown in Fig. 1, operates over a neighborhood of length 3, and can be written as:

$$c_i := c_{i-1} \vee c_{i-1} \wedge c_i \vee c_i \wedge c_{i+1} \quad (6)$$

The vector c is a vector of bits and (6) is Boolean algebra, which explains the high computational efficiency of this traffic model. Notice that (6) implies that the current state of the system is described completely by the state in the previous time step; i.e. it is Markovian and deterministic. Stochastic components are added by the signal control policy, and therefore our traffic model satisfies the main assumption of the MDP framework.

The network corresponds to a grid network of bidirectional streets with one lane per direction and with a traffic light on all intersections. To attain spatial homogeneity, the network is defined on a torus where each street can be thought of as a ring road where all intersections have 4 incoming and 4 outgoing approaches; see Fig. 2.

Vehicle routing is random: A driver reaching the stop line, say Mary, will choose to turn with probability p or keep going straight with probability $1 - p$. If Mary decides to turn, she will turn left, right or U-turn with equal probability. For instance, $p = 3/4$ gives an equal probability of $1/4$ to all possibilities and therefore promotes a uniform distribution of density on the network. If two or more vehicles are bound for the same approach during a time step, the tie is broken randomly. If the downstream approach is jammed (at jam density) then Mary will not move during that time step, and will repeat the same selection process during the next time step.

Notice that this random routing is a simplified form of driver adaptation (Gayah et al., 2014), which avoids unrealistic bifurcations in the MFD (Daganzo et al., 2011).³ It also makes our results applicable only to grid networks where both supply and demand are spatially homogeneous, e.g. where origins and destinations are uniformly distributed across the network, such as in a busy downtown CBD.

In the spirit of our discussion surrounding (1) we parametrize the space of all grid networks by λ and δ . As such, **the block length**, defined as the distance (in number of cells) between two neighboring traffic lights on a given street, is a random variable with coefficient of variation δ , while keeping its mean, ℓ , constant. Notice that values of $\ell \geq 6$ do not change simulation results.

Traffic signals operate under the simplest possible setting with only red and green phases (no lost time, red-red, yellow nor turning phases). All the control policies consider here are *incremental* in the sense that decisions are taken every g time steps, which can be interpreted as a minimum green time: After the completion of each green time of length g , the controller decides whether to prolong the current phase or to switch light colors.

The following signal control policies will be used as baseline in this paper:

1. LQF: “longest queue first” gives the green to the direction with the longest queue; it is a greedy methods for the “best” control,
2. SQF: “shortest queue first”, a greedy methods for the “worst” control,
3. RND: “random” control gives the green with equal probability to both directions, akin to no control.

The motivation to include SQF is that any possible control method will produce performance measures in between LQF and SQF.

To achieve the λ -parametrization we note from (1a) the expected green time is $E(\text{green time}) = \ell(1/u + 1/w)/\lambda$, where $(1/u + 1/w)$ is the proportionality constant in (1a), u and w are the fundamental diagram free-flow speed and wave speed, respectively, which are both equal to 1 in our scaling, so:

$$E(\text{green time}) = 2\ell/\lambda \tag{7}$$

But under incremental control the expected green time is unknown a priori; it can only be estimated after the simulation run. In particular, setting a minimum green time g in the simulation will yield $E(\text{green time}) \geq g$ due to the possibility of running two or more minimum green phases in a row. We have verified that under LQF $E(\text{green time}) \approx g$, which is as expected because after a discharge it is very unlikely that the same approach would have the largest queue. Under the random policy the number of minimum green phases in a row is described by a geometric process of probability one half, and therefore $E(\text{green time}) \approx 2g$. With this, we are able to compare LQF and RND control for a given λ by setting a minimum green time g in the simulation as:

$$g = \begin{cases} 2\ell/\lambda & \text{for LQF} \\ \ell/\lambda & \text{for RND} \end{cases} \tag{8a}$$

$$\tag{8b}$$

Unfortunately, under SQF a λ -parametrization is not possible because λ becomes ill-defined, as $E(\text{green time}) \rightarrow \infty$ for one axes and $E(\text{green time}) \rightarrow 0$ for the other; i.e., after a few iterations the signal colors becomes permanent.

³Bifurcation takes place when drivers cannot clear the intersection because the downstream link in their route is jammed. If the driver does not adapt and change her route, the jam propagates even faster, eventually leading to a deadlock, with a portion of the links in the network being jammed, and the rest being empty. With driver adaptation, however, the jam propagation is slowed down by distributing congestion more uniformly across the entire network.

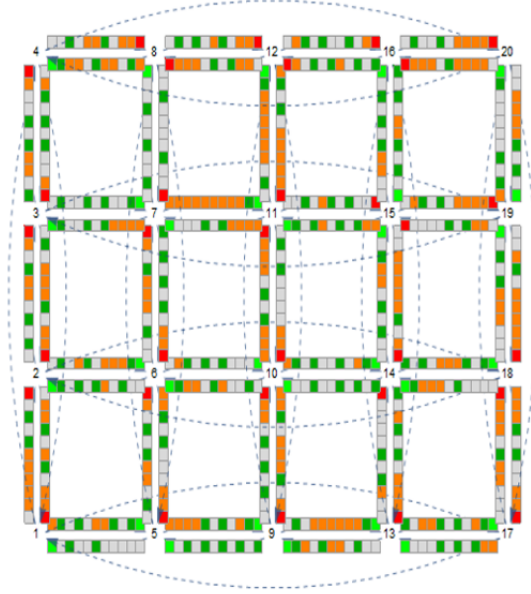


Figure 2: Example 4x5 traffic network. The connecting links to form the torus are shown as dashed directed links; we have omitted the cells on these links to avoid clutter. Each segment has $\ell = 10$ cells; an additional cell has been added downstream of each segment to indicate the traffic light color.

This is expected because after a discharge it is very likely that the same approach would have the smallest queue and therefore keep the green phase. Although this behavior is clearly unpractical, it turns out that SQF is key to understanding the behavior of DRL methods in congestion.

4. Baseline experiments

In this section we perform a series of experiments to highlight important properties of urban networks under the baseline control policies defined above. We are interested on the steady-state MFD these policies produce when deployed to all intersections in the network, and for different parameters λ , δ and p . The MFD for each policy is obtained by simulating this policy for network densities $k \in (0, 1)$ and reporting the average flow in the network after 4 cycles. This process is repeated 50 times for each density value to obtain an approximate 90%-probability interval (between the 5th and the 95th percentile) of the flow for each density value. Based on our results and to facilitates this discussion, we argue that networks have 4 distinctive traffic states: extreme free-flow ($k < 0.2$), moderate free-flow ($0.2 < k < 0.5$), moderate congestion ($0.5 < k < 0.8$) and extreme congestion ($k > 0.8$).⁴

The following results are based on 2 figures showing our simulation results for different network parameters λ , p and δ for the three baseline signal control methods. Fig. 3 shows the case of a fixed turning probability, $p = 0.75$, and different network parameters λ and δ , to make the point that the effect of δ is small. The first row corresponds to homogeneous networks (identical block lengths, $\delta = 0$), while the second row to inhomogeneous networks (highly variable block lengths, $\delta = 0.7$). Fig. 4 is for homogeneous networks ($\delta = 0$) and selected network parameter λ and p , to see the impact of turning probabilities. These figures also show the extreme cuts produced by our earlier theory in Laval and Castrillón (2015), which correspond to straight lines of slopes u_0 and w_0 given by (2).

We can draw the following remarks from Fig. 3 and 4:

⁴In traditional units of measurements we would have approximately: extreme free-flow ($k < 0.1$), moderate free-flow ($0.1 < k < 0.25$), moderate congestion ($0.25 < k < 0.7$) and extreme congestion ($k > 0.7$).

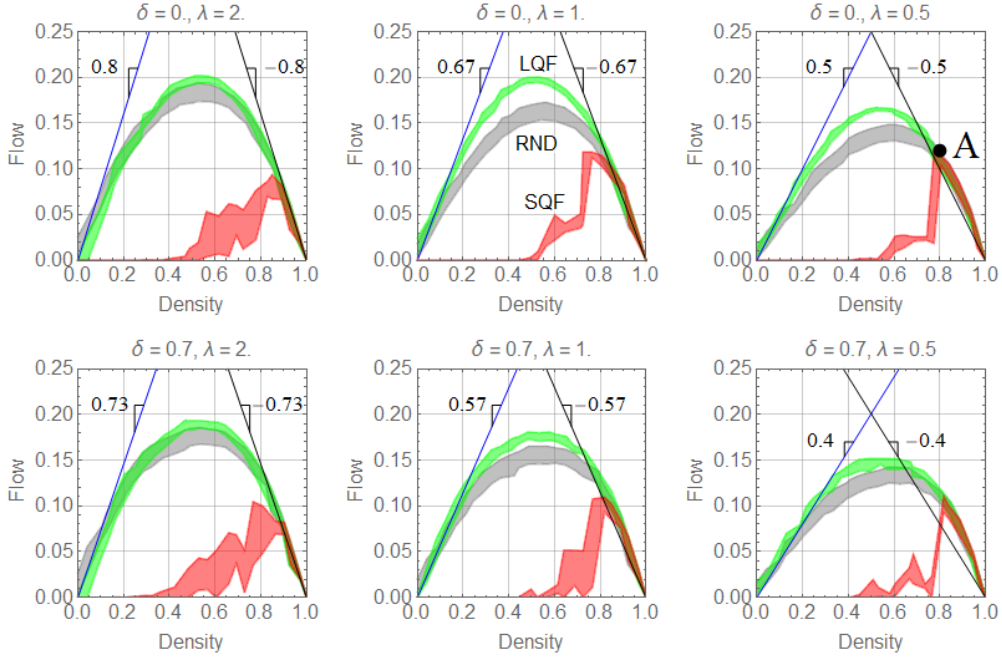


Figure 3: Simulation results for baseline policies under equally-probable turning case $p = 0.75$. First row: homogeneous networks (identical block lengths, $\delta = 0$); second row: inhomogeneous networks (highly variable block lengths, $\delta = 0.7$). The straight lines correspond to the extreme cuts in Laval and Castrillón (2015), whose slopes u_0 and $-w_0$ are given by (2).

- R-1** The block length parameter λ has a significant impact on the MFD, especially for $\lambda < 2$ and for the LQF and random control. This is as expected given that the probability of spillbacks in the network is directly related to λ .
- R-2** The variability of block length parameter δ does not impact network throughput very significantly: by comparing the diagrams in each column of Fig. 3 we can see that the shape of the MFDs is practically the same, with inhomogeneous networks producing slightly less capacity. This result is surprising and indicates that networks with highly variable block lengths with mean ℓ performs only slightly less efficiently than an idealised chess-board network with identical blocks of length ℓ . To simplify our analysis in the sequel, we now assume $\delta = 0$ unless otherwise indicated.
- R-3** Whenever LQF and RND overlap indicates that no control (i.e. RND) is an effective control method. In the flow-density plane this happens in extreme congestion and (to a lesser extent) in extreme free-flow on all networks. Consideration of (an extended version of) Fig. 4 reveals that the regions in the (λ, p) -plane where these policies overlap *for all densities* can be summarized as in the left panel of Fig. 5. It can be seen that these regions represent a significant proportion of all possible grid networks.
- R-4** There is a loss of symmetry in the MFDs for the LQF and RND policies, which can be traced to the turning probability p . From Fig. 4 we have mapped the level of skewness in the (λ, p) -plane and summarize the results in the middle and right panels of Fig. 5. It can be seen that the patterns are very different between the two policies. The precise mechanisms to explain this result will be investigated in a sequel paper.
- R-5** SQF produces permanent street colors. The middle row in Fig. 4 shows two examples where SQF flows exceed all other policies in congestion. This “detaching” behavior in the MFD happens in $p \leq 0.3$, and is a consequence of the signal color under SQF becoming permanent at each intersection. This induces a surprising collective pattern where all streets in the network are either under a permanent green and at high flows, namely “green streets”, or under permanent red and at zero flow, namely “red streets”. All green streets belong to the same axis, say N-S, which may contain some red streets; the other axis, say E-W, contains only red streets. This is shown in Fig. 6 (left), where it can be seen that the network reached an equilibrium where half of the N-S streets are

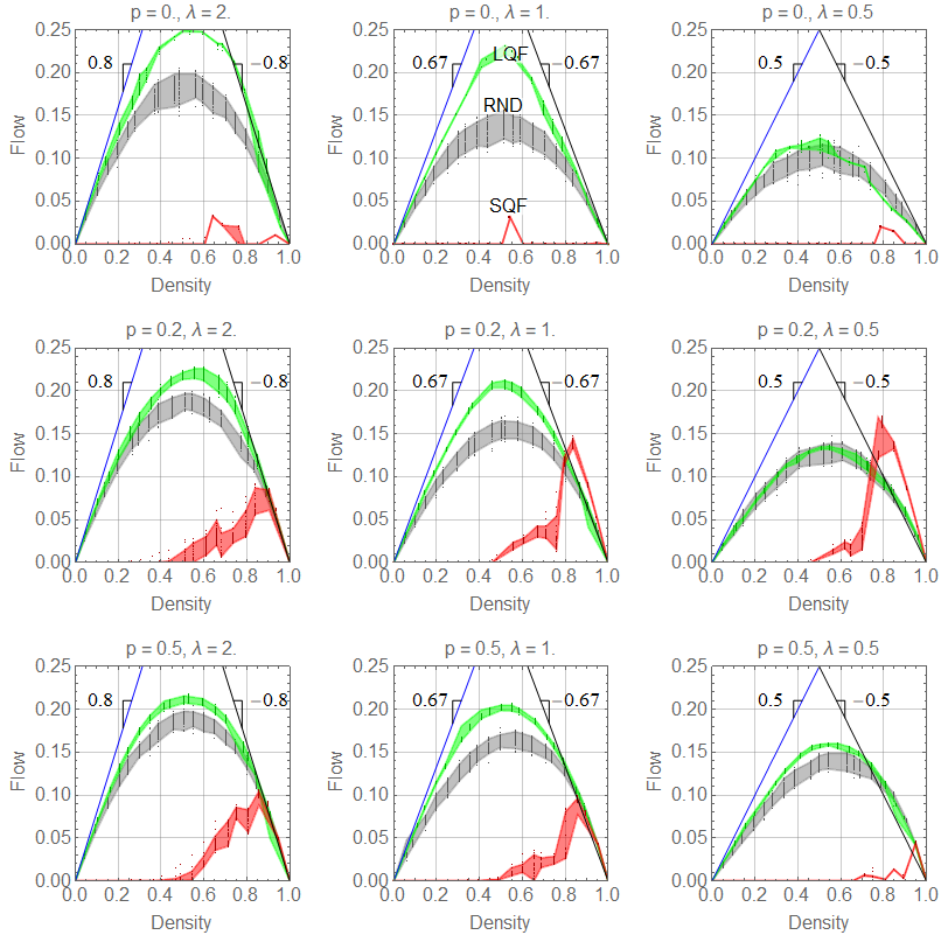


Figure 4: Simulation results for baseline policies for homogeneous networks ($\delta = 0$) and different network parameter λ (columns) and p (rows). The straight lines correspond to the extreme cuts in Laval and Castrillón (2015), whose slopes u_0 and w_0 are given by (2). Dots represent simulation points.

green, and all other streets are red. Although permanent street colors tend to emerge for all values of p , we have observed that detaching only occurs in $p \leq 0.3$, where the high flows in the green streets, shown as a green disk in the right side of the figure, are able to compensate for the zero flow in all red streets (red disk in the figure), such that the average traffic state in the network (gray disk) is above the LQF-MFD. Consideration shows that depending on the proportion of green streets the average traffic state lays anywhere within the shaded triangle in the figure, whose left edge is achieved when the proportion of green streets is maximal, i.e. 50 % in the case of square networks. Points along the line of slope $-w$ in the figure indicate that the N-S axis is operating in the congested branch of the FD, and points in the detaching area, that the N-S axis is operating in its free-flow branch. This is clearly unpractical but indicates that a good strategy under severe congestion might be to favor one axis over the other.

R-6 The congested network property: In extreme congestion LQF and RND controls always overlap, which indicates that network throughput is *independent* of traffic signal control; see point “A” in Fig. 3.

These results highlight the importance of parametrizing urban networks by λ and p because of the unique and repeatable features that emerge under particular values of these parameters. The precise mechanisms roughly outlined above are still under investigation and will be formulated on sequel papers. Here, we focus on the impact of the congested network property in **R-6** in emerging control technologies, as it shows that urban networks are more predictable than previously thought with respect to signal control. Recall from the introduction that earlier works from

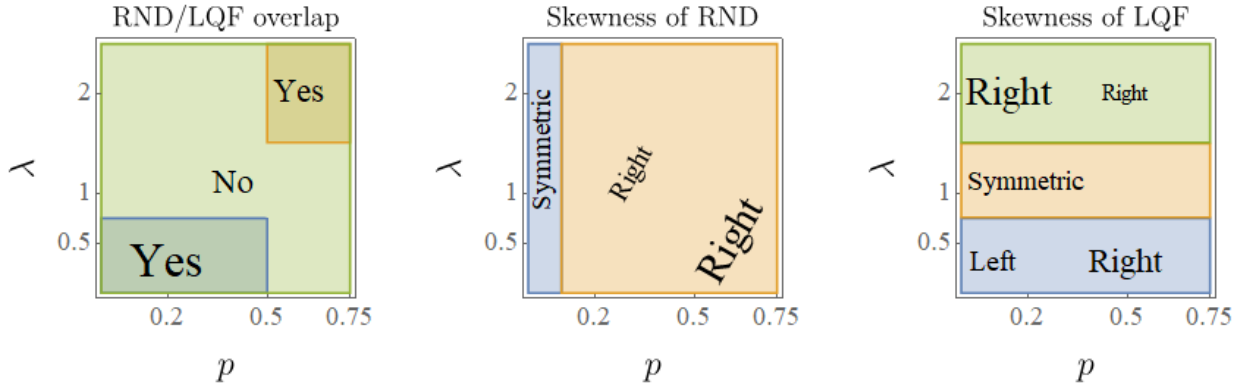


Figure 5: Summary of results in the (λ, p) -plane. Yes = LQF and RND overlap (for all densities), No = LQF and RND do not overlap, Symmetric = no skewness, Right = skewed to the right, Left = skewed to the left. The font size is proportional to the effect being shown in each panel. These diagrams are approximate and were constructed by direct observation of a large number of flow-density charts such as the ones in Fig. 4.

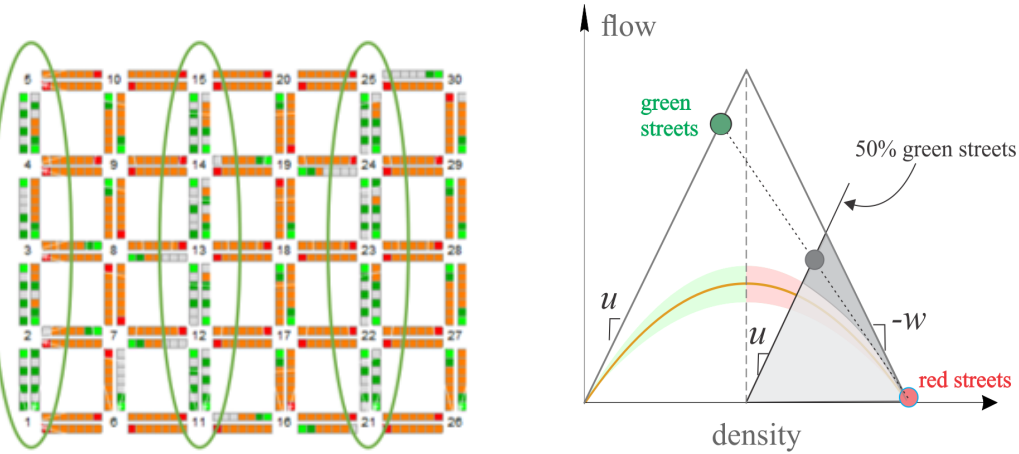


Figure 6: SQF detaching. Left: the network reached an equilibrium where half of the N-S streets are "green streets", and all other streets are "red streets". Right: low-density diagram showing the high flows in the green streets (green disk), zero flow in all red streets (red disk) and the average traffic state in the network (gray disk).

the late eighties found some evidence of the congested network property in **R-6** using simulation on a homogeneous grid network; here we have shown that this property applies even for inhomogeneous networks, and that in extreme congestion the MFD is identical across controls and network parameters.

As we will see in the next section this congested network property creates a challenge for learning effective control policies under congestion, where the policy tends to produce results similar to SQF, including detaching.

5. Machine learning experiments

In this section we perform the same experiments in the previous section but with signal control policies based on machine learning methods. Each traffic signal is an agent equipped with a deep neural network with weights θ to represent the control policy $\pi(a|s; \theta)$, as shown in Fig. 7. It is a 3-layer perceptron with tanh nonlinearity, known to approximate any continuous function with an arbitrary accuracy provided the network is "deep enough" (Kurková, 1992). The input to the network is **the state observable by the agent**: a vector of length 8, each entry representing the number of vehicles in each approach to/from the intersection. The output is a single real number that gives the probability of turning the light red for the N-S approaches (and therefore turns the light green for the E-W approaches). Recall that these actions can be taken at most every g time steps, per (8).

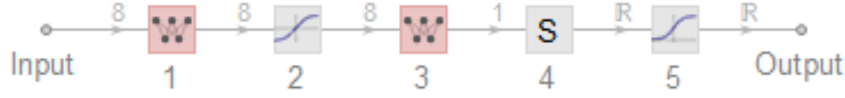


Figure 7: Neural network architecture to approximate the policy. The numbers on top of the arrows indicate the dimensions of the corresponding input/output vectors, and the numbers below the squares are as follows: the input is the state observable by the agent, 1: linear layer, 2: tanh function, 3: linear layer, 4: summation layer, 5: sigmoid function, and the output is a single real number that gives the probability of turning the light red for the N-S approaches.

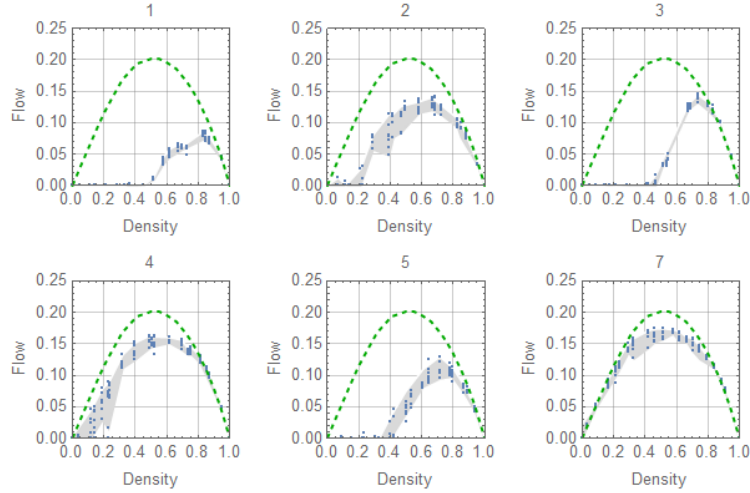


Figure 8: Random policies. Each diagram is a different trial, and shows the average density versus average flow in the network. The dashed line corresponds to the benchmark LQF policy, and dots represent simulation points. The figure assumes $\delta = 0$, $\lambda = 1$ and $p = 3/4$; we have verified that similar conclusions are obtained with other parameter values.

Because our network is spatially homogeneous and without boundaries, there is no reason why policies should be different across agents, and therefore we will train *a single agent* and share its parameters with all other agents. After training, we evaluate the performance of the policy once deployed to all agents by observing the resulting MFD. Shown in all flow-density diagrams that follow is the mean LQF policy, depicted as a thick dashed curve. In this way, we are able to test the hypotheses that the policy outperforms LQF simply by observing if the shaded area is above the dashed line. In particular, we will say that a policy is “optimal” if it outperforms LQF, “competitive” if it performs similarly to LQF, and “suboptimal” if it underperforms LQF. To train the policy we will use the following methods:

1. Random search: the weights θ for the policy are set randomly,
2. Supervised learning: given labeled data, the weights are set to minimize the prediction error,
3. Deep Reinforcement Learning (policy gradient).

The results for each of these methods are presented in the following 3 subsections.

5.1. Random search

In this experiment the weights θ for the policy are set according to a standard normal distribution. As illustrated in Fig. 8, it is possible to find a competitive policy after just a few trials; as in trial 7 in the figure. A visual analysis of a large collection of such images reveals that about 15% of these random policies are competitive.

Notice that this figure also confirms that all policies, no matter how bad, are optimal when the density exceeds approximately 75%, which is consistent with the congested network property revealed in the previous section.

5.2. Supervised learning policies

This section reports a rather surprising result: training the policy with **only two** examples yields a near-optimal policy. These examples are shown in Fig. 9 and correspond to two extreme situations where the choice is trivial: the

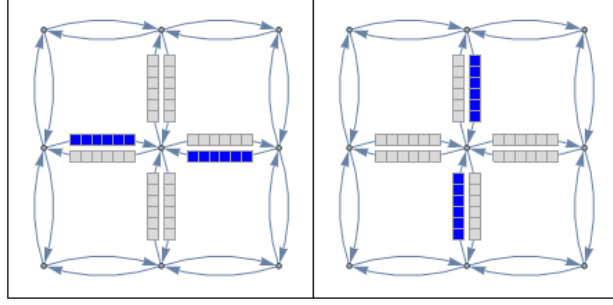


Figure 9: Supervised learning experiment. Left: Extreme state s_1 , where both N-S approaches are empty and the E-W ones are at jam density; we have omitted the cells on links other than the ones observable by the middle intersection to avoid clutter. Right: extreme state s_2 , the opposite of s_1 .

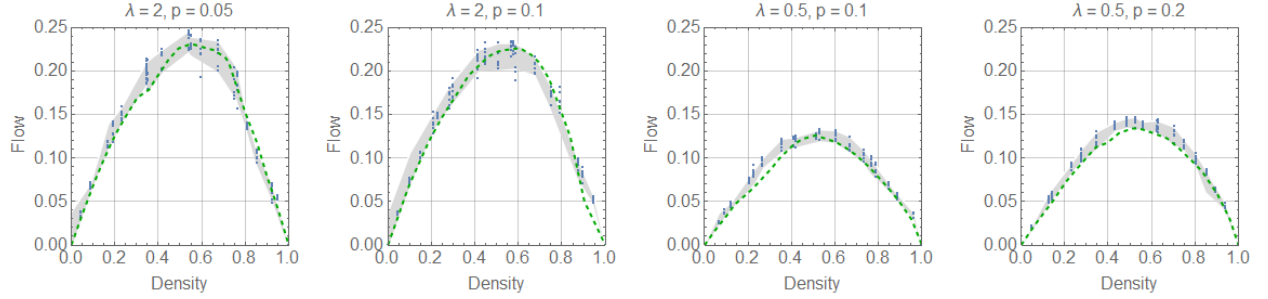


Figure 10: Supervised learning experiment: Resulting MFD (shaded area) for selected parameter values. Dots represent simulation points, and the dashed line the corresponding LQF-MFD.

left panel shows extreme state s_1 , where both N-S approaches are empty and the E-W ones are at jam density (and therefore red should be given to those approaches with probability one), while the right panel shows s_2 , the opposite situation (and therefore red should be given to N-S approaches with probability zero); in both cases all outgoing approaches are empty. The training data is simply:

$$\pi(s_1) \rightarrow 1, \quad \pi(s_2) \rightarrow 0. \quad (9)$$

We have verified that this policy gives optimal or competitive policies for all network parameters; see Fig. 10 for selected parameter values.

5.3. DRL policies

Here the policy parameters are trained using DRL on a single intersection using Algorithm 1 in the appendix. The density of vehicles in the network, k , is kept constant during the entire training process. We define **the reward** at time t , R_t , as the *average advantage flow per lane*, defined here as the average flow through the intersection during $(t, t + g)$ minus the flow predicted by the LQF-MFD at the prevailing density. In this context the LQF-MFD can be seen as a baseline for the learning algorithm, which reduces parameter variance.

The results for network parameters $\lambda = 1/2, p = 3/4$, and random initial policy weights θ are shown in Fig. 11. Each row corresponds to a constant training density k , while the first column depicts the NS red probabilities of the extreme states, $\pi(s_1)$ and $\pi(s_2)$ (described in section 5.2) as a function of the iteration number, and these probabilities should tend to (9) for “sensible” policies. To facilitate the discussion, let DRL-F be a DRL policy trained under free-flow conditions, i.e. $k < 0.5$ and DRL-C under congestion, i.e. $k \geq 0.5$. We can see from Fig. 11 that:

1. DRL-F policies are only competitive, with lower training densities leading to policies closer to LQF.
2. DRL-C policies are suboptimal and deteriorate as k increases. Sensible policies cannot be achieved for training density $k \geq 0.7$ as probabilities $\pi(s_1)$ and $\pi(s_2)$ converge to the SQF values; see the first column in Fig. 11.

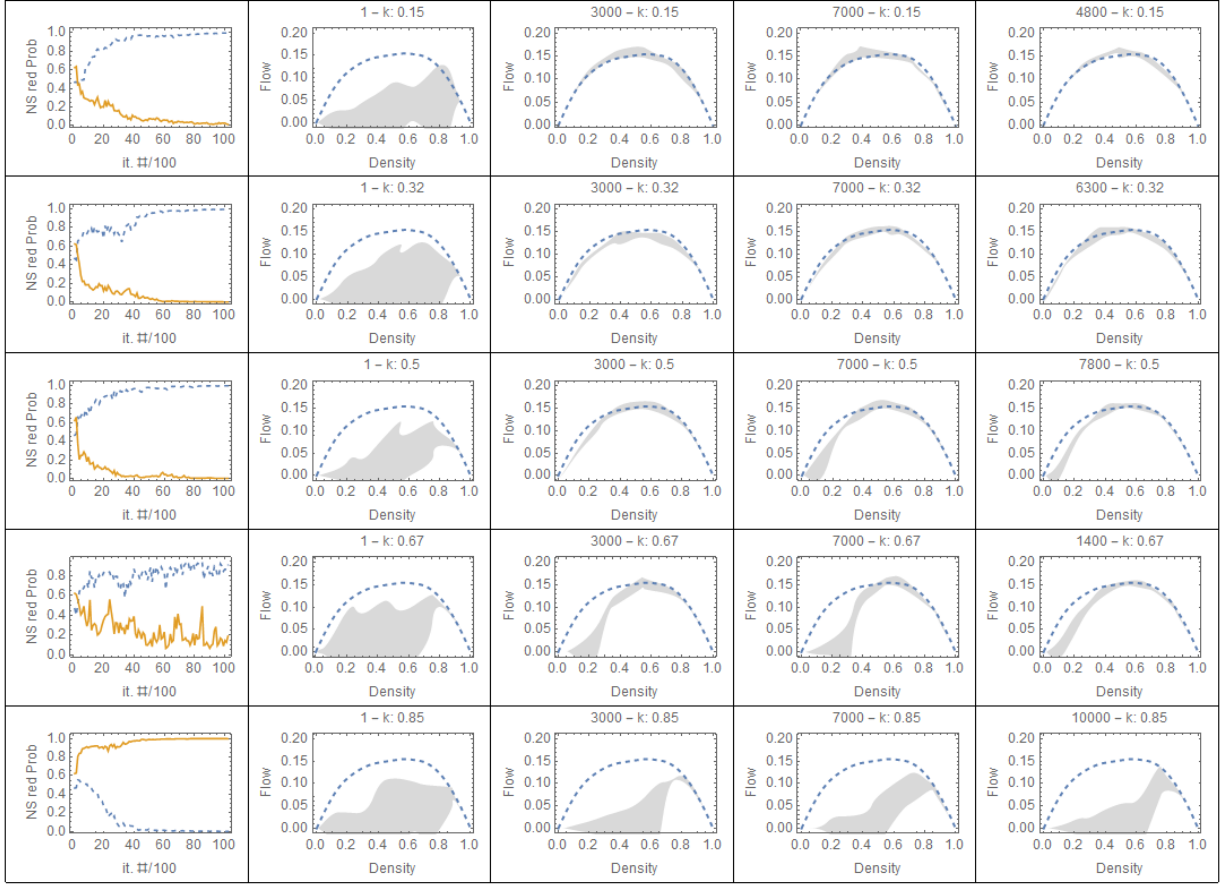


Figure 11: Policies trained with constant demand and random initial parameters θ with $\lambda = 1/2$ and equally likely turning probability $p = 3/4$. The label in each diagram gives the iteration number and the constant density value. First column: NS red probabilities of the extreme states, $\pi(s_1)$ in dashed line and $\pi(s_2)$ in solid line. The remaining columns show the flow-density diagrams obtained at different iterations, and the last column shows the iteration producing the highest flow at $k = 0.5$, if not reported on an earlier column.

These observations indicate that DRL policies are only competitive and lose their ability to learn a sensible policy as the training density k increases. This is consistent with the congested network property, whereby the more the congestion, the less the policy affects intersection throughput. This can make the DRL-C gradient $\nabla_{\theta} \log \pi \rightarrow 0$ for $p \geq 0.5$, not because an optimal policy has been reached but because there is nothing to be learned at that density level; see Fig. 13. Notice that for lower turning probabilities the tendency of the DRL-C gradient is similar to the other panels in the figure, but still the probabilities $\pi(s_1)$ and $\pi(s_2)$ converge to the SQF values.

While the above findings are true for all network parameters, it is important to note that DRL can outperform LQF in some cases. In $0.05 \leq p \leq 0.2$, $\lambda < 1$ detaching is learned by (i) DRL-F with random initial weights, and by (ii) DRL-F and DRL-C with optimal weights given by supervised learning. That DRL-F can learn detaching is surprising since at that training density level ($k < 0.5$) detaching does not take place. Not so for DRL-C because we have shown that it tends to SQF. The DRL detaching behavior is even more pronounced than SQF, which indicates that the number of “green streets” obtained by this policy is higher than under SQF. This improvement upon SQF is unexpected and indicates that DRL is able to learn how to outperform LQF in congestion, albeit impractically since signal colors become permanent.

This is shown in Fig. 14, where the first panel shows how the resulting MFD detaches from the LQF-MFD, in a way consistent with our explanation in Fig. 6. The remaining panels show simulation results with the same policy but with higher turning probabilities during simulation, p_{sim} in the figure. It can be seen that the detaching decreases with p_{sim} eventually disappearing for $p_{\text{sim}} \geq 0.3$, at which point the network is subject to the congested network property.

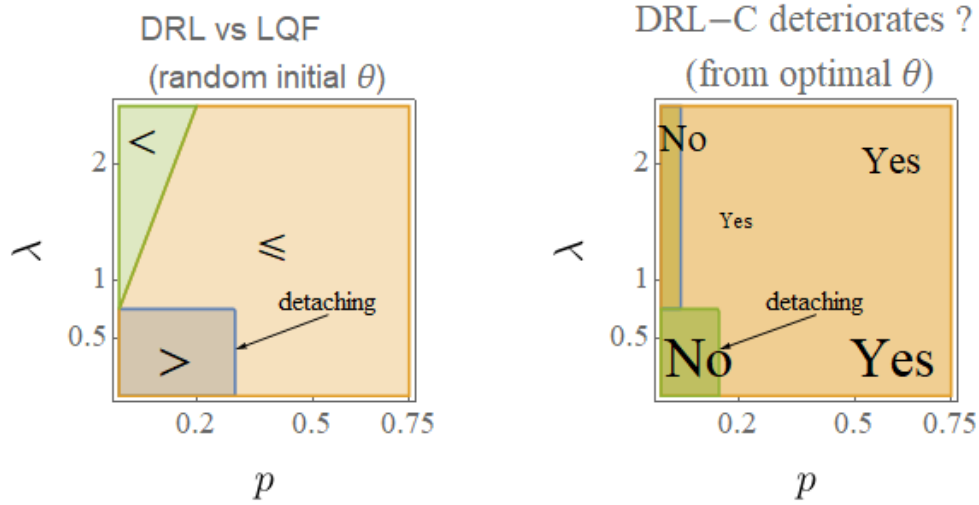


Figure 12: Summary of results in the (λ, p) -plane. Left: regions where, starting from random initial parameters, the “best” DRL policy (across training densities) performs better ($>$), worse ($<$) or comparable to (\approx) LQF. Right: regions where the DRL policy trained in congestion deteriorates, starting with optimal parameters. The font size is proportional to the effect being shown in each panel.

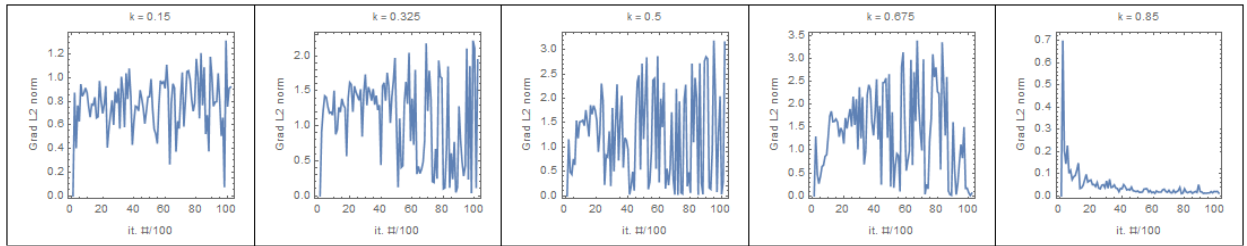


Figure 13: Evolution of the gradient L_2 -norm $\|\nabla_{\theta} \log \pi\|_2$ as a function of the iteration number. The gradient goes to zero not because an optimal policy has been reached but because all actions yielded similar throughput near point “A” in Fig. 3.

Finally, Fig. 12 shows a summary of results in the (λ, p) -plane. The left panel shows the regions where the DRL policy trained at any density and starting from random initial parameters performs better ($>$), worse ($<$) or comparable to (\approx) LQF. It can be seen that except for detaching, the general policy always underperforms LQF. The right panel shows the regions where the DRL policy trained in congestion deteriorates, starting with optimal parameters from the supervised experiment. Again, except for detaching and when $p = 0$, the additional DRL training under congested conditions leads to a deterioration of the policy, which increases with p .

6. Discussion and outlook

This paper exposed several important properties of urban networks, which have remained unnoticed until now, and that have important implications for traffic control. While a sequel paper will explore the theoretical aspects of these properties, here we focused on their impact on machine learning methods applied to traffic signal control on large networks. Recall that our results apply to all grid networks with origins and destinations uniformly distributed across the network.

Our main result is the congested network property: on congested urban networks the intersection throughput tends to be independent of signal control. We conjecture that this prevents DRL methods from finding sensible policies under congested conditions and learn SQF instead. Even starting with initial weights given by the supervised training policy, we saw that additional training under congested conditions leads to a deterioration of the policy. We have verified similar behavior under dynamic demand loads whenever congestion appears in the network. This means, potentially, that all the DRL methods proposed in the literature to date are unable to learn sensible policies and

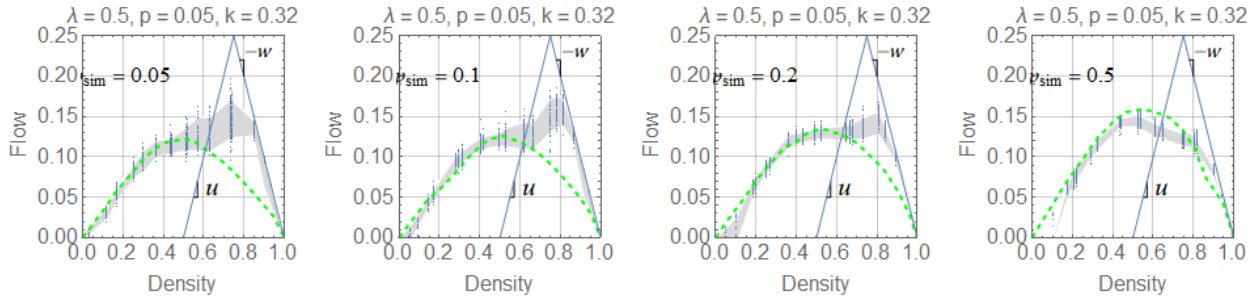


Figure 14: Detaching policy found by DRL. Each panel shows simulation results with the same policy but with different turning probabilities during simulation, p_{sim} . Dashed line: LQF-MFD for $\lambda = 0.5, \delta = 0$ and p_{sim} . The straight lines are included to facilitate the comparison with our explanation in Fig. 6.

deteriorate as soon as congestion appears on the network. It might also explain DRL’s limited success for traffic signal control problems observed so far, currently believed to be due to urban networks being non-stationary and/or non-Markovian (Choi et al., 2000, Da Silva et al., 2006). We believe instead that the congested network property is to blame, and that future work should focus on new DRL methods able to extract relevant knowledge from congested conditions. In the meantime, it is advisable to train DRL policies under free-flow conditions only, discarding any information from congested ones, as we have shown here that such free-flow DRL policies are comparable to LQF.

That DRL learns LQF in free-flow indicates that most of what the agent needs to learn, e.g. flushing the longest queue, is encoded in free-flow conditions. This is intuitive because in free-flow there are no spillbacks and thus the reward grows linearly with the state variable. Less intuitive is that in congestion DRL consistently learns SQF. Since the gradient information is not useful due to the congested network property, one would expect that it learns RND instead. Why this happens remains an open question, and might hold the clue to improving DRL methods in congestion.

We have shown that networks with different parameters λ, p and to a much lower extent δ , exhibit very different responses to traffic signal control, and it is therefore imperative to parameterize them by at least λ and p . While the congested network property is true for all networks, other properties are not. Notably, we found that no control (i.e. random policy) can be an effective control strategy for a surprisingly large family of networks. Fig. 5 summarizes the experiments in Figs. 3 and 4, where one can see that in roughly 1/3 of the cases the MFD for LQF and RND policies overlap for any density level.

The impact of the turning probability p turned out to be very significant, not only for explaining the behavior of baseline policies but also for endowing DRL to find policies that exceed SQF’s ability to produce the detaching phenomenon introduced in this paper. Albeit unpractical, detaching strongly suggest that an excellent strategy under severe congestion might be to favor one axis over the other. The case $p \rightarrow 0$ can be problematic in the current framework because the environment tends to be deterministic, which contradicts the assumptions of the type of stochastic gradient descent methods traditionally used in DRL. We observed that for $p < 5\%$ competitive DRL policies are hard to find. Turning probabilities also explain the loss of symmetry observed for LQF and RND baseline policies, which is not captured by existing theories that rely on corridor approximations without turns. Unveiling the mechanisms for the loss of symmetry due to turning should provide significant insight into the operation of urban networks. It becomes clear that future research should focus on mapping the origin and destination table and dynamic traffic assignment models to turning probabilities.

Notably, we also found that supervised learning with only two examples yields optimal or near-optimal policies for all network parameter values. This intriguing result indicates that extreme states s_1 and s_2 encode vital information and that the neural network can successfully extrapolate to all other states. Understanding precisely why this happens could lead to very effective supervised learning methods based on expert knowledge, and perhaps to supplement DRL’s inability to learn under congested conditions.

Although not shown in the main text, we have verified that other state representations have little impact on the resulting machine learning policies. Besides from a vector of length 8 used in the main text as input to the neural net, where each entry represents the number of queued vehicles in each approach to/from the intersection, we also tried (i)

a vector of length 4 only considering incoming approaches, (ii) a $8 \times \ell$ matrix of bits, given the four incoming and the four outgoing c -vectors from the CA model, one for each approach to/from the intersection, and (iii) a $4 \times \ell$ matrix only considering incoming approaches. Considering all 8 approaches to/from the intersection would make it possible for the model to learn to avoid spillbacks. But according to the main result in this paper, this might have not happened. Instead, we found that with the $8 \times \ell$ input (but not the $4 \times \ell$) supervised learning yields a near-optimal policy with only two examples. This is surprising because the outgoing approaches are simply null vectors in these two examples used for training, but somehow the larger configuration endows the model with better extrapolation capabilities.

A crucial assumption in this work was driver adaptation to avoid bifurcations in the MFD, which has not been observed in the field to the best of our knowledge. Without driver adaptation a different DRL framework would have to be used with the reward function having to capture the possibility of localized gridlocks and the state observable by the agent having to capture their spatial extent. The agent might also need to learn the origin-destination matrix since gridlock probabilities grow with the number of nearby origins and destinations. All the questions raised in this discussion are currently being investigated by the authors.

Finally, we have verified that the results in this paper remain true under more realistic network configurations and other DRL training algorithms. This is shown in the appendix using the the open-source microscopic traffic simulator SUMO (Krajzewicz et al., 2012), where we have also included an open Github repository.

Acknowledgements

The authors are grateful to Hani Mahmassani for pointing out the studies from the mid-eighties mentioned in the introduction. This study has received funding from NSF research projects # 1562536 and # 1932451.

Appendix A. The training algorithm REINFORCE-TD

In this paper we propose the training algorithm REINFORCE-TD, which is in the spirit of REINFORCE with baseline (Williamms, 1988) but for continuing problems. To the best of our knowledge, this extension of REINFORCE is not available in the literature, which is almost entirely focused on episodic problems as discussed earlier. Notice that we tried other methods in the literature with very similar results, so REINFORCE-TD is chosen here since it has the fewest hyperparameters: learning rates α and β for weights, θ , and average reward, $\eta(\pi)$, respectively. Using a grid search over these hyperparameters resulted in $\alpha = 0.2$ and $\beta = 0.05$.

Recall that REINFORCE is probably the simplest policy gradient algorithm that uses (4) to guide the weight search. In the episode setting it is considered a Monte-Carlo method since it requires full episode replay, and it has been considered to be incompatible with continuing problems in the literature (Sutton and Barto, 2018). Here, we argue that a one-step Temporal Difference (TD) approach (Sutton, 1988) can be used instead of the Monte-Carlo replay to fit the continuing setting. This boils down to estimating the differential return (5) by the temporal one-step differential return of an action:

$$G_t \approx R_t - \eta(\pi) \tag{A.1}$$

Notice that the second term in this expression can be interpreted as a baseline in REINFORCE, which are known to reduce weight variance. The pseudocode is shown in Algorithm 1.

Appendix B. Results using SUMO

We include this appendix to highlight that the results presented here can be replicated and extended using the the open-source microscopic traffic simulator SUMO (Krajzewicz et al., 2012).

All DRL settings are kept as in the main text, except for the state representation, which corresponds here to a vector containing the queue lengths of each lane approaching the intersection. For training, we implemented both REINFORCE-TD and the more advanced policy gradient algorithm A2C (Actor to Critic) for the continuing setting in Sutton and Barto (2018), and we obtained similar results. Fig B.16 shows the (untransformed) SUMO experiment results for the 3 baseline policies studied here and for a DRL policy trained under congested conditions (DRL-C) using REINFORCE-TD. It can be seen that these results are consistent with the model in the main text.

The project is open on Github:https://github.com/zhouhao0605/signal_control_paper

Algorithm 1 REINFORCE-TD

- 1: Input: weighted policy $\pi(a|s; \theta)$, $\theta \in \mathcal{R}^m$, average density k
 - 2: Set hyper-parameter α, β , set average reward $\eta = 0$
 - 3: Initialize vector θ
 - 4: Initialize the network state S as a Bernoulli process with probability k over the cells in the network
 - 5: **repeat**
 - 6: Generate action $A \sim \pi(\cdot|S; \theta)$
 - 7: Take action A , observe the new state S' and reward R (by running the traffic simulation model for g time steps)
 - 8: $G \leftarrow R - \eta$
 - 9: $\eta \leftarrow \eta + \beta G$
 - 10: $\theta \leftarrow \theta + \alpha G \nabla_{\theta} \log \pi(A|S; \theta)$
 - 11: $S \leftarrow S'$
 - 12: **until** forever
-

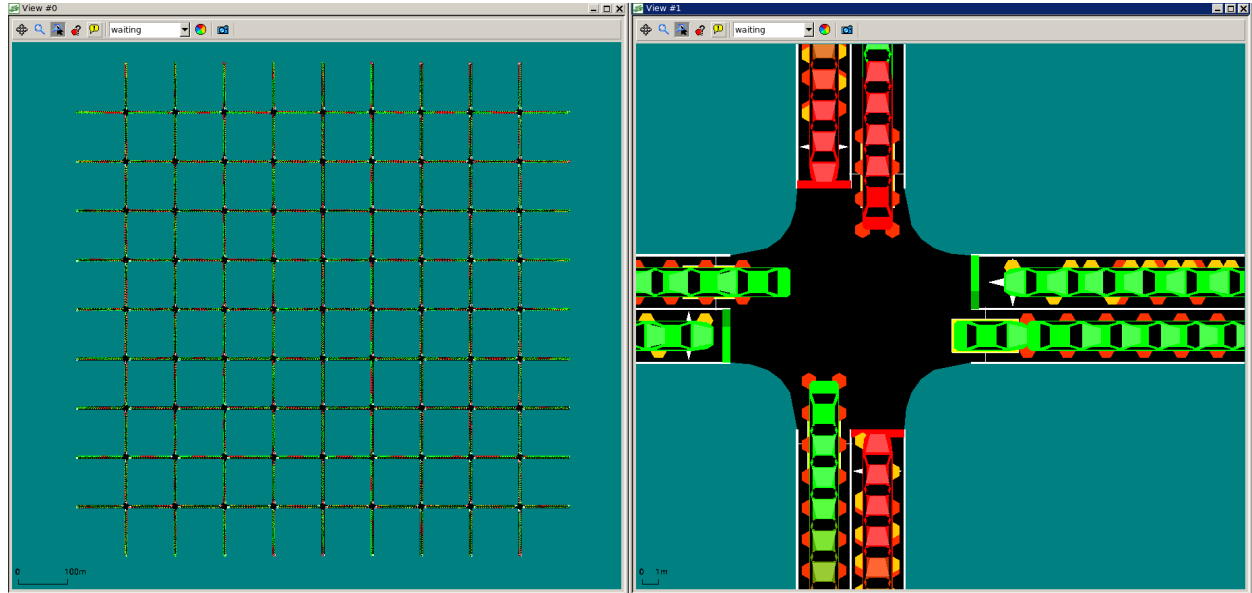


Figure B.15: A 9*9 grid network in SUMO: All roads are one-lane, traffic lights are two-phase without protected left-turns. $\lambda = 4.0$ and $\delta = 0$. Vehicles randomly turn at intersections and make U-turn at boundaries. Notice that we modified the default routing algorithm in SUMO to achieve high density level without gridlock. Internal links of intersections are removed and downstream spill-back are prevented.

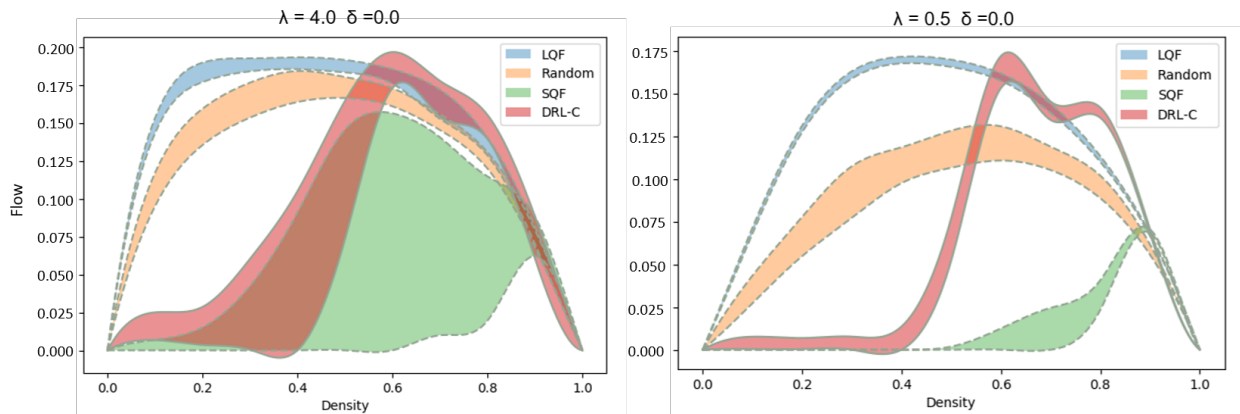


Figure B.16: MFD of DRL-C and baseline policies: Upper and lower envelopes correspond to the 95% and 5% percentiles of average network flow from 100 trails. Red shaded area depicts the MFD of DRL-C in extreme congestion (density 0.9). Curves are derived through interpolation from discrete point values at density 0.1,0.2,...,0.9.

References

- Adewumi, A., Kagamba, J., Alochukwu, A., 2016. Application of chaos theory in the prediction of motorised traffic flows on urban networks. *Mathematical Problems in Engineering*.
- Arel, I., Liu, C., Urbanik, T., Kohls, A., 2010. Reinforcement learning-based multi-agent system for network traffic signal control. *IET Intelligent Transport Systems* 4, 128–135.
- Belletti, F., Haziza, D., Gomes, G., Bayen, A.M., 2017. Expert level control of ramp metering based on multi-task deep reinforcement learning. *IEEE Transactions on Intelligent Transportation Systems* 19, 1198–1207.
- Bellman, R., 1957. A markovian decision process. *Journal of mathematics and mechanics*, 679–684.
- Bertsekas, D.P., 1987. *Dynamic Programming: Determinist. and Stochast. Models*. Prentice-Hall.
- Camponogara, E., Kraus, W., 2003. Distributed learning agents in urban traffic control, in: *Portuguese Conference on Artificial Intelligence*, Springer. pp. 324–335.
- Chen, J., Yuan, B., Tomizuka, M., 2019. Model-free deep reinforcement learning for urban autonomous driving. *arXiv preprint arXiv:1904.09503*.
- Choi, S.P., Yeung, D.Y., Zhang, N.L., 2000. Hidden-mode markov decision processes for nonstationary sequential decision making, in: *Sequence Learning*. Springer, pp. 264–287.
- Chu, T., Qu, S., Wang, J., 2016. Large-scale traffic grid signal control with regional reinforcement learning, in: *2016 American Control Conference (ACC)*, IEEE. pp. 815–820.
- Chu, T., Wang, J., 2015. Traffic signal control with macroscopic fundamental diagrams, in: *2015 American Control Conference (ACC)*, IEEE. pp. 4380–4385.
- Chu, T., Wang, J., Codecà, L., Li, Z., 2019. Multi-agent deep reinforcement learning for large-scale traffic signal control. *IEEE Transactions on Intelligent Transportation Systems*.
- Da Silva, B.C., Basso, E.W., Bazzan, A.L., Engel, P.M., 2006. Dealing with non-stationary environments using context detection, in: *Proceedings of the 23rd international conference on Machine learning*, ACM. pp. 217–224.
- Daganzo, C.F., 1996. The nature of freeway gridlock and how to prevent it. *Transportation and traffic theory*, 629–646.
- Daganzo, C.F., 1998. Queue spillovers in transportation networks with a route choice. *Transportation Science* 32, 3–11.
- Daganzo, C.F., Gayah, V.V., Gonzales, E.J., 2011. Macroscopic relations of urban traffic variables: Bifurcations, multivaluedness and instability. *Transportation Research Part B: Methodological* 45, 278–288.
- Daganzo, C.F., Geroliminis, N., 2008. An analytical approximation for the macroscopic fundamental diagram of urban traffic. *Transportation Research Part B: Methodological* 42, 771–781.
- Dai, Y., Hu, J., Zhao, D., Zhu, F., 2011. Neural network based online traffic signal controller design with reinforcement training, in: *2011 14th International IEEE Conference on Intelligent Transportation Systems (ITSC)*, IEEE. pp. 1045–1050.
- Gayah, V.V., Gao, X.S., Nagle, A.S., 2014. On the impacts of locally adaptive signal control on urban network stability and the macroscopic fundamental diagram. *Transportation Research Part B: Methodological* 70, 255–268.
- Ge, H., Song, Y., Wu, C., Ren, J., Tan, G., 2019. Cooperative deep q-learning with q-value transfer for multi-intersection signal control. *IEEE Access* 7, 40797–40809.
- Genders, W., Razavi, S., 2016. Using a deep reinforcement learning agent for traffic signal control. *arXiv preprint arXiv:1611.01142*.
- Godfrey, J., 1969. The mechanism of a road network. *Traffic Engineering & Control* 8.
- Gong, Y., Abdel-Aty, M., Cai, Q., Rahman, M.S., 2019. A Decentralized Network Level Adaptive Signal Control Algorithm By Deep Reinforcement Learning. *Technical Report*.
- Herman, R., Ardekani, S., 1984. Characterizing traffic conditions in urban areas. *Transportation Science* 18, 101–140.
- Herman, R., Prigogine, I., 1979. A two-fluid approach to town traffic. *Science* 204, 148–151.

- Howard, R.A., 1960. Dynamic programming and markov processes. .
- Khamis, M.A., Gomaa, W., 2014. Adaptive multi-objective reinforcement learning with hybrid exploration for traffic signal control based on cooperative multi-agent framework. *Engineering Applications of Artificial Intelligence* 29, 134–151.
- Kheterpal, N., Parvate, K., Wu, C., Kreidieh, A., Vinitzky, E., Bayen, A., 2018. Flow: Deep reinforcement learning for control in sumo. *SUMO* , 134–151.
- Krajzewicz, D., Erdmann, J., Behrisch, M., Bieker, L., 2012. Recent development and applications of SUMO - Simulation of Urban MObility. *International Journal On Advances in Systems and Measurements* 5, 128–138. URL: <http://elib.dlr.de/80483/>.
- Kurková, V., 1992. Kolmogorov's theorem and multilayer neural networks. *Neural networks* 5, 501–506.
- Laval, J.A., Castrillón, F., 2015. Stochastic approximations for the macroscopic fundamental diagram of urban networks. *Transportation Research Procedia* 7, 615–630.
- Laval, J.A., Chilukuri, B.R., 2016. Symmetries in the kinematic wave model and a parameter-free representation of traffic flow. *Transportation Research Part B: Methodological* 89, 168 – 177.
- Li, L., Lv, Y., Wang, F.Y., 2016. Traffic signal timing via deep reinforcement learning. *IEEE/CAA Journal of Automatica Sinica* 3, 247–254.
- Lighthill, M.J., Whitham, G.B., 1955. On kinematic waves ii. a theory of traffic flow on long crowded roads. *Proceedings of the Royal Society of London. Series A. Mathematical and Physical Sciences* 229, 317–345.
- Lillicrap, T.P., Hunt, J.J., Pritzel, A., Heess, N., Erez, T., Tassa, Y., Silver, D., Wierstra, D., 2015. Continuous control with deep reinforcement learning. arXiv preprint arXiv:1509.02971 .
- Mahmassani, H., Herman, R., Walton, M., 1985. Characterizing the Evolution of Urban Patterns and Traffic Network Performance. Technical Report.
- Mahmassani, H.S., Jayakrishnan, R., Herman, R., 1990. Network traffic flow theory: Microscopic simulation experiments on supercomputers. *Transportation Research Part A: General* 24, 149–162.
- Mahmassani, H.S., Williams, J.C., Herman, R., 1984. Investigation of network-level traffic flow relationships: some simulation results. *Transportation Research Record* 971, 121–130.
- Mnih, V., Kavukcuoglu, K., Silver, D., Rusu, A.A., Veness, J., Bellemare, M.G., Graves, A., Hiedmiller, M., Fiedjeland, A.K., Ostrovski, G., et al., 2015. Human-level control through deep reinforcement learning. *Nature* 518, 529.
- Nair, A.S., Liu, J.C., Rilett, L., Gupta, S., 2001. Non-linear analysis of traffic flow, in: *ITSC 2001. 2001 IEEE Intelligent Transportation Systems. Proceedings (Cat. No. 01TH8585)*, IEEE. pp. 681–685.
- Puterman, M., 1994. Markovian decision problems.
- Richards, P.I., 1956. Shock waves on the highway. *Operations research* 4, 42–51.
- Silver, D., Schrittwieser, J., Simonyan, K., Antonoglou, I., Huang, A., Guez, A., Hubert, T., Baker, L., Lai, M., Bolton, A., et al., 2017. Mastering the game of go without human knowledge. *Nature* 550, 354.
- Smeed, R.J., 1967. The road capacity of city centers. *Highway Research Record* .
- Sutton, R., 1999. The policy process: an overview. Overseas Development Institute London.
- Sutton, R.S., 1988. Learning to predict by the methods of temporal differences. *Machine learning* 3, 9–44.
- Sutton, R.S., Barto, A.G., 2018. *Reinforcement learning: An introduction*. MIT press.
- Tan, T., Bao, F., Deng, Y., Jin, A., Dai, Q., Wang, J., 2019. Cooperative deep reinforcement learning for large-scale traffic grid signal control. *IEEE transactions on cybernetics* .
- Vinitzky, E., Kreidieh, A., Le Flem, L., Kheterpal, N., Jang, K., Wu, F., Liaw, R., Liang, E., Bayen, A.M., 2018. Benchmarks for reinforcement learning in mixed-autonomy traffic, in: *Conference on Robot Learning*, pp. 399–409.
- Wei, H., Xu, N., Zhang, H., Zheng, G., Zang, X., Chen, C., Zhang, W., Zhu, Y., Xu, K., Li, Z., 2019. Colight: Learning network-level cooperation for traffic signal control. arXiv preprint arXiv:1905.05717 .
- Williams, J., Mahmassani, H., Herman, R., 1985. Analysis of traffic network flow relations and two-fluid model parameter sensitivity. *Transportation Research Record* , 95–106.
- Williamns, R., 1988. Toward a theory of reinforcement-learning connectionist systems. Technical Report NU-CCS-88-3, Northeastern University .
- Wolfram, S., 1984. Cellular automata as models of complexity. *Nature* 311, 419.
- Xu, M., Wu, J., Huang, L., Zhou, R., Wang, T., Hu, D., 2018. Network-wide traffic signal control based on the discovery of critical nodes and deep reinforcement learning. *Journal of Intelligent Transportation Systems* , 1–10.